HYDRODYNAMIC DESIGN OF THE FASTRAC TURBOPUMP

Roberto Garcia and Robert Williams
NASA
Fluid Dynamics Division
Marshall Space Flight Center, AL

Shawn Fears
NASA
Propulsion Systems Division
Marshall Space Flight Center, AL

ABSTRACT

A 60,000 lb thrust, liquid Oxygen (LOX) and rocket propellant #1 (RP-1) rocket engine is being developed at the Marshall Space Flight Center (MSFC) as part of NASA's ongoing effort to lower the cost of access to space. The goal of the program is to demonstrate a low cost rocket engine with acceptable performance. In order to reduce design and development risk, computational fluid dynamics (CFD) analysis was used extensively in the design process, especially in the design of the turbopump. This paper documents the process used and significant results obtained during the design of the LOX and RP-1 pumps. This includes the design of the inlet manifolds, the integral inducer-impellers, the diffusers, and the collector volutes. The resulting designs incorporate low-cost design features while meeting the engine cycle requirements.

INTRODUCTION

As part of NASA's ongoing effort to lower the cost of access to space, MSFC is developing a 60,000 lb thrust rocket engine that will demonstrate significantly lower recurring cost than rocket engines currently in use. The gas generator (GG) cycle engine, known as the Fastrac engine, uses LOX and RP-1 for propellants. In addition to low recurring cost, there are also ambitious goals associated with the development schedule and cost. These cost and schedule constraints made it imperative that sophisticated design tools be employed as early as possible in the design process, and, whenever possible, commercially available off-the-shelf (COTS) components and manufacturing processes be utilized. These cost and schedule goals became requirements when the engine was chosen to power the X-34 experimental vehicle. This paper documents how CFD was used in the design of the Fastrac turbopump's LOX and RP-1 pumps.

The Fastrac turbopump (Fig. 1) is comprised of a single stage LOX pump, a single stage RP-1 pump, and a single stage supersonic turbine, all three elements on a common shaft. The LOX pump has a single axial inlet which is preceded by approximately seven inches (approximately two pump inlet diameters) of straight ducting. The RP-1 pump inlet manifold has two inlets which are supplied from a common, larger line upstream of the turbopump. The performance requirements for the pumps are shown in Table 1. Other turbopump configurations were studied. These included single shaft designs with the turbine between the two pumps, and dual shaft designs with separate turbines driving each pump. Using existing turbomachinery was also studied. While each of these options had some advantages, the single shaft configuration with the RP-1 pump between the turbine and the LOX pump was deemed to have the least development risk (both at the turbopump and engine system levels) and the lowest manufacturing cost. The team also determined that while there are turbopumps available that could meet the performance requirements, there are none available that meet the cost goals.

The cost of the turbopump is greatly affected by the pump design because of the cost associated with the two pump rotors and with the two pump housings. Therefore, in order to minimize the cost of the turbopump, it is necessary to design these pump components to be as inexpensive to manufacture as possible. Early in the program it was determined that for a small production batch it would be less expensive to machine the housings rather than to cast

Table 1. Pump performance requirements

	LOX	RP-1
Inlet pressure (psia)	34.7	21.9
Inlet temperature (^{o}R)	166.0	530.0
Flow rate (lbm/sec)	138.8	64.2
Discharge pressure (psia)	895.0	962.0

them. Therefore, the flow paths in the housings were designed to be easily machined. Later in the program it was decided that it would be beneficial to design for the use of castings in the turbopump housings since a production engine would probably use castings to lower recurring costs. Fortunately, the features that allowed for ease of machining generally also facilitated casting development.

To reduce casting development cost, the design needs to be open to one side (i.e., no internally trapped casting cores). The cross-section of the flow passages must be as large as possible, thus less stringent surface roughness and dimensional tolerance specifications are required. The cross-sectional shape should be simple for ease of pattern development, and any airfoil shapes (i.e., the volute's cutwater) should have generous leading edges that will fill easily when pouring. These manufacturing requirements are in conflict with certain performance requirements. While the relative importance of cost and performance has been reversed for the Fastrac engine, performance is still a very important factor.

Historically, for rocket engines, weight minimization has been required. Hence, designs have tended towards narrow passages with relatively high fluid velocities leading to stringent surface roughness and dimensional tolerance specifications. It is also desirable to maximize engine specific impulse (I_{sp}), which for a GG-cycle engine like the Fastrac, implies that pump efficiency should be as high as possible. Therefore, the passage cross-section in typical rocket engine turbopumps is designed to minimize losses rather than to simplify manufacturing. Airfoil shapes tend to have thin leading edges which complicate and increase the cost of manufacturing.

To reduce weight, rocket engine turbomachinery rotors typically have high rotational speeds. This means that flow entering a rotating element should be as uniform as possible to reduce dynamic loads on the rotor and that pressure distributions, especially in the collectors, be as uniform as possible to reduce the radial loads on the bearings. Thin leading edges at shallow angles are desired for inducers to maximize shaft speed. However, this leading edge nearly always rules out casting as a manufacturing method and often leads to very high machining costs. While the Fastrac rotors will be machined, consultation with the machinists led to the setting of leading edge angles and thickness that could be readily machined. In order to reduce machining costs, the number of blades at the impeller exit was reduced to levels below those recommended by traditional methods.

APPROACH

In order to reduce the developmental risk associated with these seemingly contradictory requirements, the turbopump design team elected to use CFD analysis within the design cycle. The program budget did not contain sufficient resources to improve the initial design through iterative design-and-test cycles as has been done historically. Since MSFC has been actively applying CFD analysis in the design process (Garcia et. al., 1994a, McConnaughey et. al., 1994, Garcia et. al., 1994b), sufficient experience existed for including CFD in the iterative design process. The design process was initiated by performing trade studies using a one-dimensional (1D) meanline code which yielded the initial velocity triangles and the initial sub-component size. Custom codes were then used to generate the three-dimensional (3D) surface definitions for the major flow paths in both pumps and in the turbine. These 3D surfaces were then used to generate the analysis grids. The grids were generated using Gridgen (Steinbrenner and Chawnee, 1996), TIGER (Shih, 1997), and custom codes. Gridgen is a general
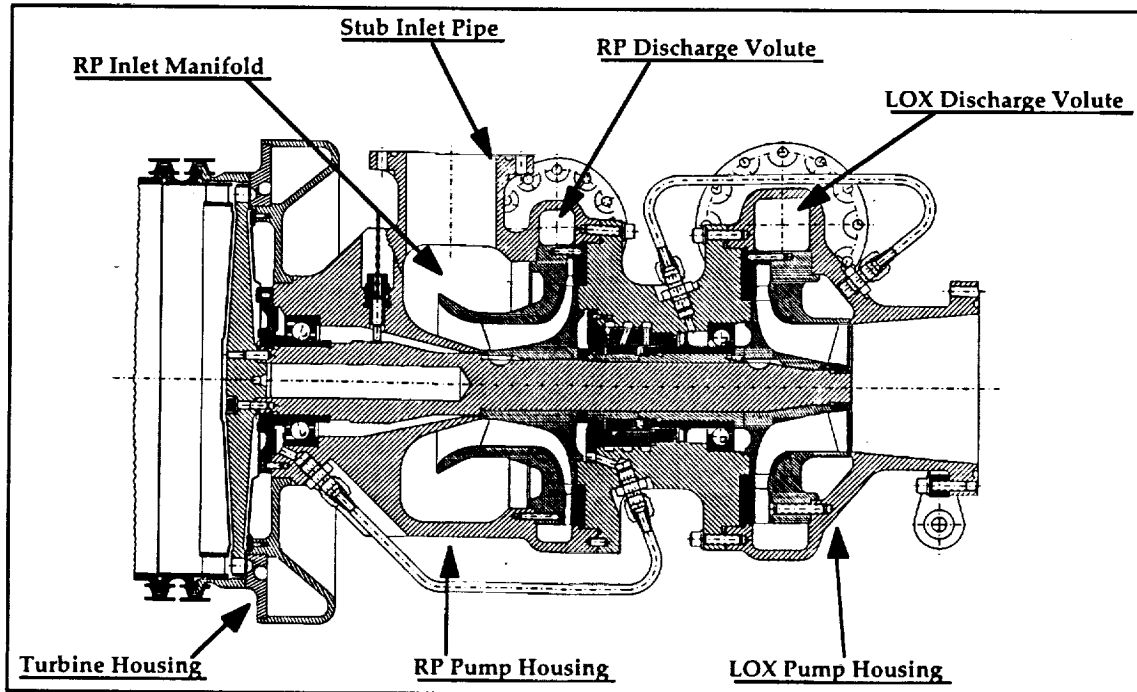

Figure 1. Fastrac tubopump cross-section

Table 2. Pump geometry and performance paramaters

	LOX	RP-1
Rotational speed, rpm	20,000	20,000
Specific speed, rpm(gpm)^0.5/ft^.75	2049	1326
Inlet flange total pressure, psi	46.0	28.0
Inlet manifold:		
inlet area, square inches		8.823
flow path outer diameter, in.		7.188
inducer annulus outer diameter, in.		4.460
inducer annulus axial gap, in.		0.900
Rotor:		
number of blades	3+6	3+6
inlet total pressure, psi	46.0	25.0
NPSP available, psi	29.3	25.0
NPSP capability, psi	22.2	13.2
inlet tip diameter, in.	3.300	3.200
inlet hub diameter, in.	1.250	1.800
inlet tip flow coefficient	0.135	0.120
leading edge tip thickness, in.	0.012	0.012
exit tip diameter, in.	4.460	5.100
exit blade span, in.	0.430	0.180
exit blade angle, degrees	26.5	41.0
total pressure rise coefficient	0.437	0.501
static pressure rise coefficient	0.295	0.313
efficiency	0.830	0.858
exit relative flow angle, degrees	14.5	20.4
exit absolute flow angle, degrees	13.9	15.1
flow split about splitter, %	54.3 - 45.7	53.3 - 46.7
Radial Diffuser:		
inner diameter, in.	4.520	5.160
outer diameter, in.	6.000	6.400
axial gap, in.	0.430	0.180
static pressure recovery coefficient	0.378	0.309
total pressure loss coefficient	0.059	0.079
Volute:		
axial depth, in.	1.375	0.915
throat area, in.	2.664	1.240
sideload,lb.	32.4	38.7
sideload angle, from cutwater	158	76
Exit diffuser cone:		
cone angle, degrees	6.00	6.3
length-to-inlet radius ratio	5.00	9.30
exit diameter	2.645	2.624
static pressure recovery coefficient	0.706	0.861
total pressure loss coefficient	0.044	0.047

purpose grid generation code initially developed under NASA sponsorship and currently being developed further by Pointwise, Inc. Gridgen's multi-block capability, geometry database capability, and grid smoothing utilities made it a very efficient tool for generating the grids for the inlet and exit manifolds. TIGER, being developed under NASA sponsorship, is very efficient at generating grids for vaned passages. It allows the user to generate the grid for complex 3D flow passages interactively on two-dimensional (2D) cascade and profile projections. Once a suitable grid was available, the CFD code FDNS (Chen, 1989) was used to obtain the flow field. FDNS is a public domain code developed under NASA sponsorship by. The features that make it suitable for use in the design process are numerical robustness, ease of problem set-up, engineering accuracy with relatively coarse grids, and extensive experience with the code among MSFC personnel. The solutions were interrogated using the public domain visualization tool FAST. Engineering information was extracted from the solution using custom codes and compared to the requirements and constraints. If the design met all the requirements then the process was considered complete, otherwise another cycle was performed.

Pre- and post-processing was the done on a Silicon Graphics (SGI) Personnel Iris (PI) workstation. Numerical solutions were computed on either a Cray T90 or an SGI Power Challenge computer. A typical design iteration would require 1.0 to 1.5 days for the inducer-impeller and 2.0 to 4.0 days for the manifolds. The manifold grids tended to be much larger than the rotor grids and, consequently, required more labor and computer time. The most labor intensive part of the design iteration process was the geometry and grid generation portion. To reduce the work required, in some cases simplifications were made to the geometry to allow as much automation in the grid generation process as possible. For example, the diffuser cone at the exit of the volutes were replaced by rectangular diffusers of equal area distribution. Once the final design was obtained, the actual cone diffuser was included in the model and the calculation was repeated. None of the simplifications used were found to significantly affect the component's performance.

One of the advantages of generating these complex models and performing these detailed calculations early in the design process is that information is readily available to improve the efficiency and depth of analysis in other areas of the design process. For example, the 3D blade shapes were readily transferred to the mechanical design group and subsequently made available to the machine shop for tool path programming. Also, the blade loads were available and were transferred (along with the geometry definition) to the structural analysis group for their assessment.

RESULTS AND DISCUSSION

General design guidelines used in the design of the pumps can be found in Huzel and Huang (1992), Furst (1973), and Jakobsen (1971). Key geometric parameters for the resulting geometry are shown in Table 2. The shaft speed of 20,000 rpm is a compromise between the desire to increase shaft speed to improve turbine efficiency (and hence I_{sp}) and the need to keep the pump's required suction specific speed (Nss) at a level that could be achieved within the cost and schedule constraints. The predicted Nss capability for the LOX and RP-1 rotors is shown in Fig. 2 as a function of the flow coefficient (f) ratio. The model used to make these predictions is on the work of Brophy (1975). This model was used to set the inducer inlet area, number of blades, leading edge thickness, and leading edge blade angle. Limits on these blade definition parameters were set by structural and manufacturing concerns.

LOX Pump Results

The LOX pump has an axial inlet and thus does not require an inlet manifold. The final integral inducer-impeller design is shown in Fig. 3. The ID code yielded the inlet and exit diameters, an estimate of the required number of blades in the impeller section, and an estimate of the impeller exit velocity triangle. A single piece inducer-impeller arrangement was selected to improve performance and simplify manufacturing and assembly. Because of this arrangement, the inducer suction requirements set the inlet velocity triangle and blading definition. Within the 3D design
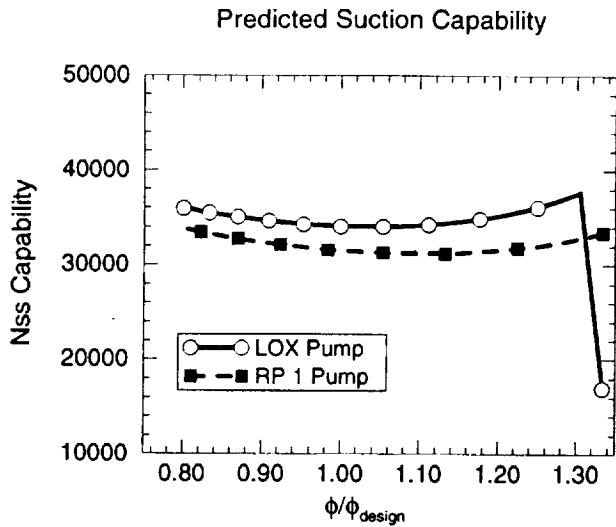
Predicted Suction Capability

Figure 2. Predicted inducer suction capability

Blade Angle Distributions

Figure 4. Blade angle distribution for the impellers

optimization iterations, the blade chordwise thickness distribution, the blade angle distribution, and the impeller profile shape were modified. The number of blades in the impeller section was not changed during the LOX pump 3D design iterations, neither was the exit diameter changed from that resulting out of the 1D parametrics.

A total of six optimization iterations were performed for the LOX inducer-impeller. The overall, mass-averaged performance parameters are listed in Table 2. The velocity contours and vectors near the hub of the rotor are shown in Fig. 3. There is no flow separation within the rotor passages when operating at the design point. The vaneless radial diffuser downstream of the impeller was included in the inducer-impeller analyses model. The leakage paths between the impeller outer diameter and the casing inner diameter
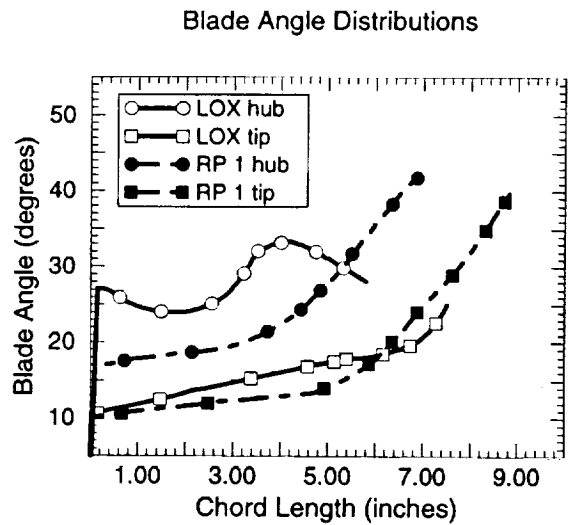
are not modeled. The final blade angle distribution along the hub and blade tip is shown in Fig. 4. This distribution is a compromise between the required head rise, the desire to minimize the overhung impeller's axial length, and ease of manufacture issues. Figure 5 shows the mass-averaged pressure rise through the rotor. Note that the majority of the pressure rise occurs in the impeller section. From these results, we can also obtain information regarding the radial diffuser. It should be noted that any interactions between the radial diffuser and the volute that might affect diffuser performance would not be captured by the rotor analysis. Although there are areas where improvements can be made to the geometry, the final design meets the system requirements and is within the design constraints.
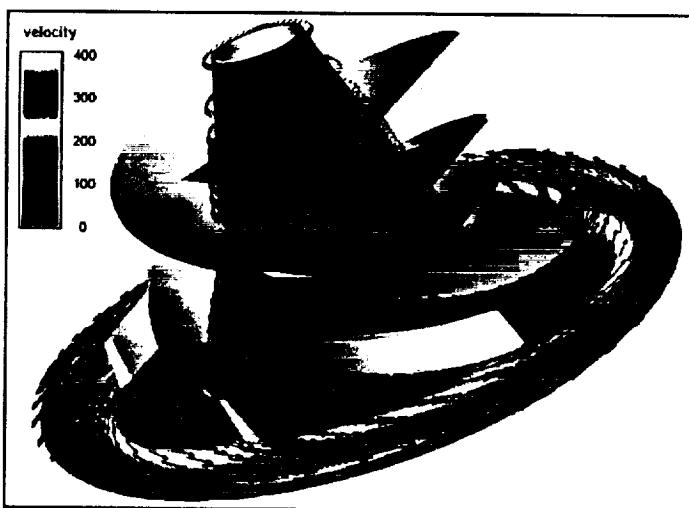

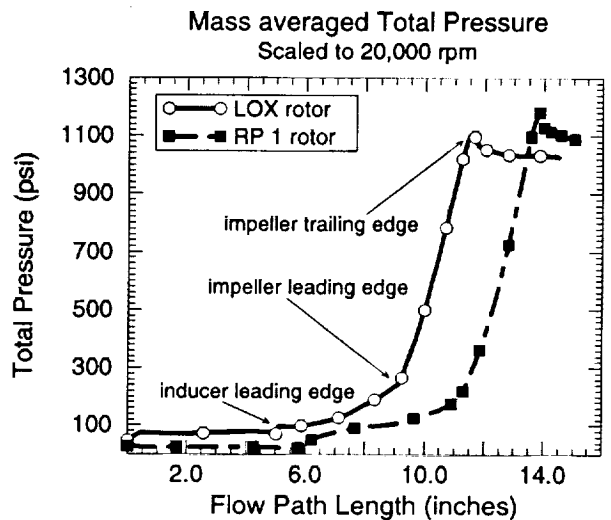**Figure 3. Velocity magnitude and vectors near the hub of the LOX Impeller**

Mass averaged Total Pressure
Scaled to 20,000 rpm

Figure 6. Total pressure rise through the Impellers
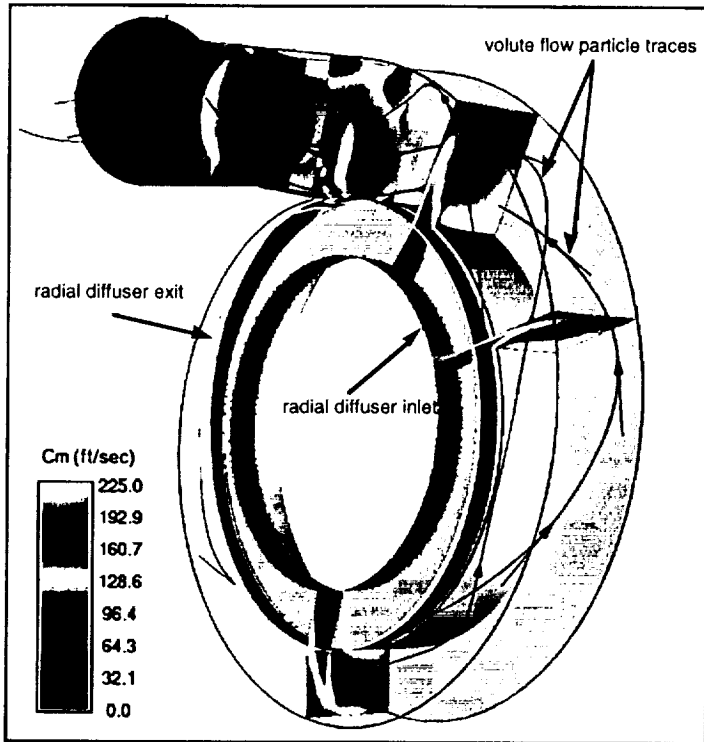
Figure 6. LOX pump volute velocity at selected planes

Cm (ft/sec)
225.0
192.9
160.7
128.6
96.4
64.3
32.1
0.0

Radial Diffuser Inlet P_{static} Variation
Scaled to 20,000 rpm

LOX, 80% ϕ_{design}
LOX, 100% ϕ_{design}
LOX, 120% ϕ_{design}
RP 1, 100% ϕ_{design}

Figure 7. Radial diffuser inlet static pressure variation

The radial vaneless diffuser, the volute collector, and the exit cone diffuser were included in the model for the collector system. Results for the final LOX pump collector design are shown in Fig. 6. The overall, mass-averaged performance for the collector system is listed in Table 2. A vaned radial diffuser was initially baselined due to structural concerns. Other solutions were eventually found for the structural concerns and the simpler vaneless diffuser was baselined for both pumps. The inlet boundary condition for the radial diffuser was based on the mass-averaged impeller exit flow angle (Table 2). It was assumed that over the limited flow range studied (the Fastrac engine does not throttle), there is no interaction between the volute and the impeller.

The volute is a constant velocity, log-spiral design with a rectangular cross-section of constant width. The discharge area for the exit cone was set by the requirement to interface with a COTS valve at the pump exit flange. A small performance penalty results due to larger than optimal diffusion. However, the exit diffuser does not separate even when operating at 80% of the design ϕ. One of the key goals of the volute design is to minimize the radial loads that the volute imposes on the
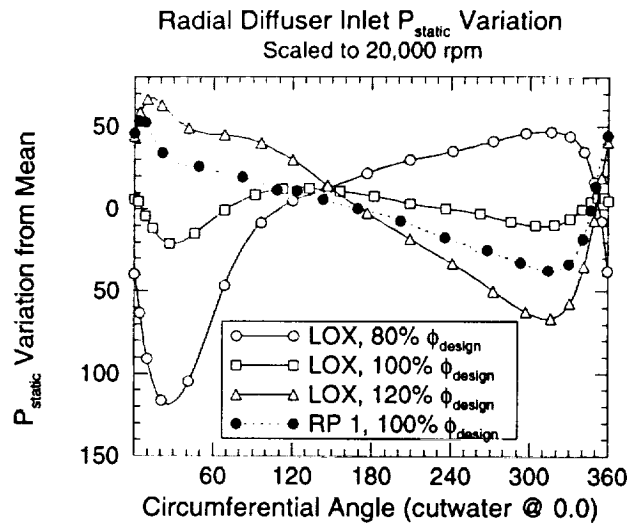
bearing system. Figure 7 shows the predicted static pressure distributions at the inlet to the radial diffuser and the resulting radial loads for operation at 20,000 rpm. These loads can be supported by the COTS bearings being used in the turbopump. The LOX pump performance will verified using a highly instrumented, water flow test rig at MSFC.
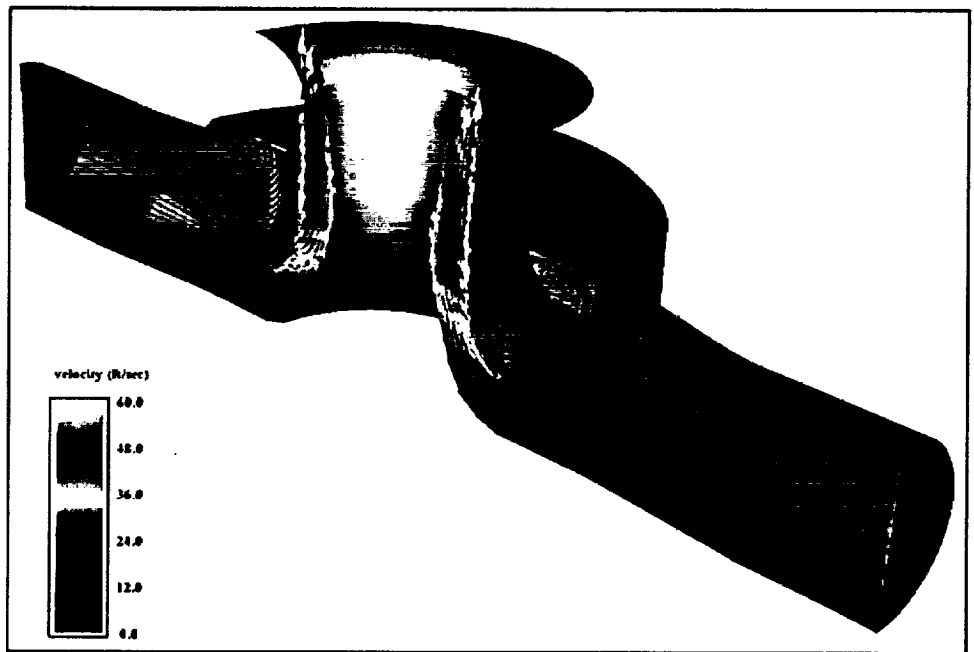

velocity (ft/sec)
60.0
48.0
36.0
24.0
12.0
0.0

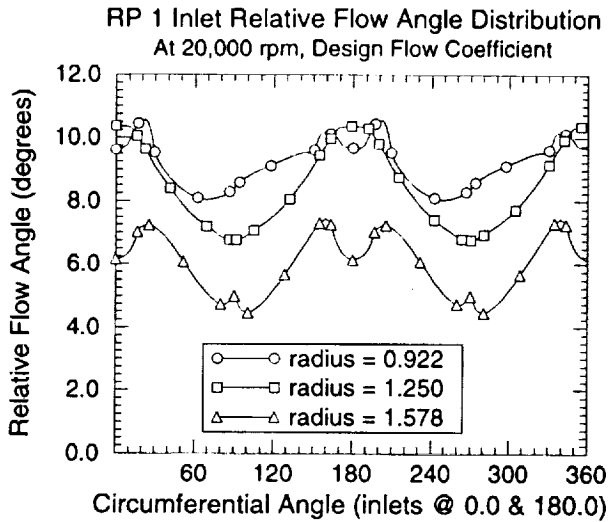**Figure 8. RP-1 pump inlet manifold showing velocity vectors on the plane of symmetry**

Figure 9. RP-1 inducer inlet relative flow
angle distribution

RP-1 Pump

The RP-1 pump requires a manifold inlet due its placement in the turbopump layout. The design of the inlet manifold consumed the most time of any of the pump sub-components, with a total of 18 designs being evaluated. Details of the design iterations for the inlet manifold can be found in Garcia (1996). The inlet manifold was designed to minimize losses and inducer inlet circumferential distortion while to retaining ease of manufacture. The resulting manifold geometry is shown in Fig. 8 with some key geometric parameters quantified in Table 2. Single inlet designs were generated and evaluated. However, in order to meet the design requirements an excessively large (and heavy) plenum volume was required. The resulting design incorporates two inlets, diametrically opposed, a mixing plenum, and an accelerating
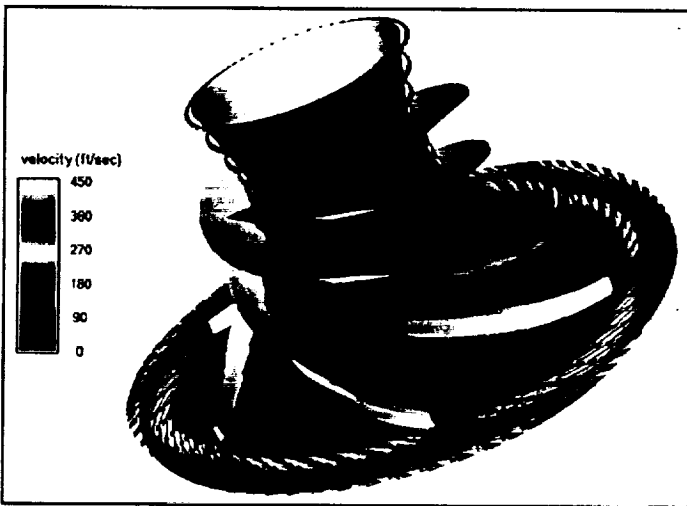

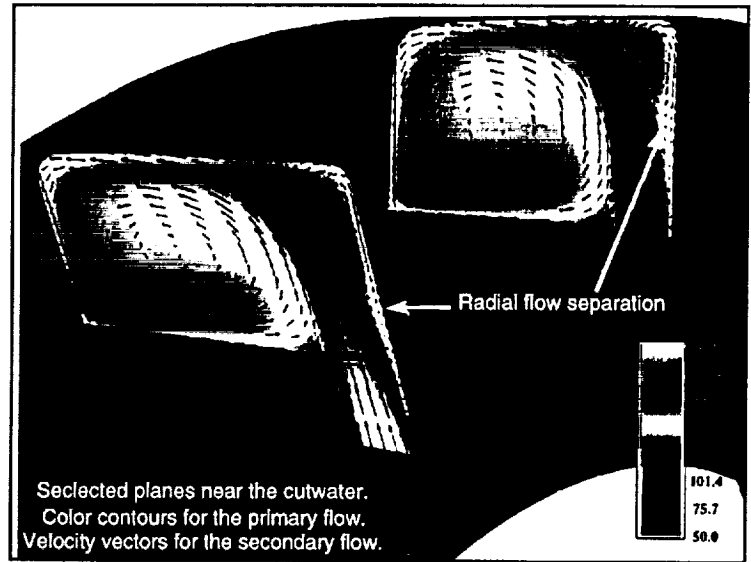Figure 10. Velocity magnitude and vectors near the
hub of the RP-1 impeller

Figure 11. Primary and secondary flow in the RP-1
volute

annulus section immediately upstream of the inducer (Fig. 1 and Fig. 8). The geometric definition of the accelerating annulus was found to be very important in achieving a successful design. The resulting RP-1 inducer inlet relative flow angle circumferential distribution is shown in Fig. 9. This distribution was mass averaged along radial lines to obtain the averaged radial flow angle profile entering the RP-1 inducer.

The final RP-1 integral inducer-impeller design (iteration#5) is shown in Fig. 10. Despite having a lower specific speed, the overall efficiency for the RP-1 rotor is higher than for the LOX rotor due a larger profile bend radius for the RP-1 rotor. It was possible to do this because there was no requirement to minimize the axial length of the RP-1 impeller. Therefore, smoother blade angle distributions (Fig. 4) were possible which consequently improved overall efficiency. The final design contains six blades at the impeller exit. The initial design, which was based on traditional design criteria, had an additional set of splitters, yielding a total of 12 blades at the impeller exit. However, elimination of the last set of splitters and slightly increasing the exit blade angle (to account for additional slip with the last set of splitters removed) netted an acceptable design. The rotor mass-averaged pressure rise is shown is Fig. 5. The rollover seen in the static pressure at the exit of the model is not a design deficiency but rather a result of a reduced area section purposely added to the model downstream of the vaneless radial diffuser.

The analysis model for the RP-1 collector system included the radial diffuser, the collector volute, and the exit cone diffuser. Six design iterations were performed before an acceptable design was obtained. The vaneless, constant axial gap radial diffuser was modeled with a fixed inlet flow angle obtained from the impeller analysis. While it was assumed that there is no interaction between the impeller and the volute, there is interaction between the radial diffuser and the volute (Fig. 11). The secondary flow in the volute tends to separate the flow on one wall of the radial diffuser, reducing
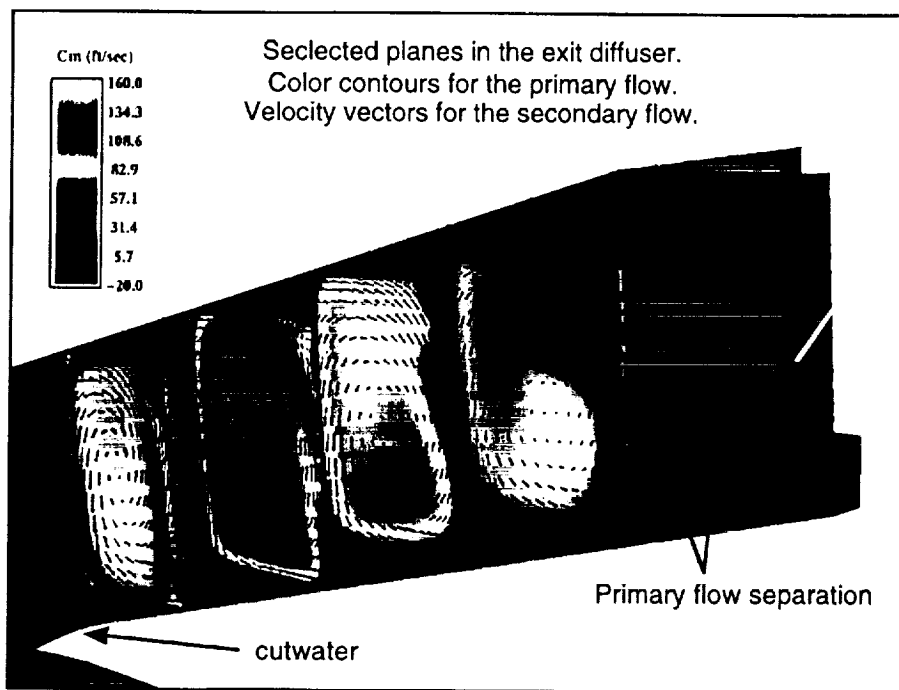
6

Figure 12. RP-1 manifold exit diffuser flow pattern. Rectangular diffuser shown.

its effective area. This same phenomenon manifested itself in the LOX pump. By generating the image shown in Fig. 11 at different circumferential stations around the volute, it was possible to determine that the separation is due to the interaction between the radial diffuser and the volute rather than due to diffuser stall.

The RP-1 pump volute design philosophy was similar to that used for the LOX volute. Geometric and performance parameters for the RP-1 volute can be found in Table 2. [Note: off-design calculations for the RP-2 collector system will available by Dec. 1997] The resulting static pressure distribution at the radial diffuser inlet (Fig. 7) indicates that the RP-1 volute is slightly undersized. However, the resulting radial loads and performance are acceptable. The exit of the cone diffuser is required to interface with the same size COTS valve as the LOX pump. This requirement, along with limits on the cone angle, led to a large length-to-throat radius ratio for the exit diffuser. The result is a stall of the cone diffuser (Fig. 12). The stall seems to be driven by the secondary flow generated by the volute which tends to accumulate the low energy flow in one quadrant of the exit diffuser. Attempts to eliminate this stall with ribs and vanes were not successful. The design was accepted based on the rational that the separation occurs in a region of relatively low dynamic pressure (approximately 13 psi); thus exacting a small performance penalty. The risk for system instabilities being initiated by this separation was judged to low. Both the RP-1 pump and the LOX pump will be tested at the turbopump level with the actual propellants (initial tests will use liquid Nitrogen instead of LOX) prior to engine level testing.

CONCLUSION

During the design of the Fastrac turbopump, extensive use was made of CFD analysis. The 3D design of the LOX and RP-1 pumps was done with CFD analysis included in the iterative design process. This has allowed the incorporation of cost saving features into the turbopump design without sacrificing performance. The integral inducer-impellers incorporate wide passages and a brazed shroud to simplify machining thus lowering cost. The manifolds incorporate open passages and rectangular flow path cross-sections to facilitate either machining or casting.

REFERENCES

Brophy, M. C., 1975, "A Theoretical Study of Cavitating Inducers With an Application to Water-Jet Propulsion," Research and Development Report 4431, February 1975, Naval Ship Research and Development Center, Bethesda, MD.

Chen, Y. S., 1989, "Compressible and Incompressible Flow Computations with a Pressure Based Method," AIAA 89-0286, AIAA 27th Aerospace Meeting and Exhibit, Jan. 9-12, Reno, NV.

Furst, R. B., 1973, "NASA Space Vehicle Design Criteria (Chemical Propulsion), Liquid Rocket Engine Centrifugal Flow Turbopumps," NASA SP 8109, December 1973.

Garcia, R., McConnaughey, P., Eastland, A., 1994a, "Computational Fluid Dynamics Analysis for the Reduction of Impeller Discharge Flow Distortion," AIAA 94-0749, AIAA 32nd Aerospace Meeting and Exhibit, Jan. 10-13, Reno, NV.

Garcia, R., Griffin, L., Benjamin, T., Cornelison, J., Ruf, J., Williams, R., 1994b, "Computational Fluid Dynamics Analysis in Support of the Simplex Turbopump Design," *Proceedings of the 1994 Conference on Advanced Earth-to-Orbit Propulsion Technology*, NASA CP-3282, R. J. Richmond and S. T. Wu, eds., May 17-19, Marshall Space Flight Center, AL, Vol. 1, pp. 462-470.

Garcia, R., 1996, "Fluid Analysis of Pump Manifolds Designed for Cost," JANNAF Propulsion Meeting, December 9-13, Albuquerque, NM.

Huzel, D. K., Huang, D. H., 1992, *Modern Engineering for Design of Liquid-Propellant Rocket Engines*, AIAA Progress in Astronautics and Aeronautics, Vol. 147, pp. 155-218.

Jacobsen, J. K., 1971, "NASA Space Vehicle Design Criteria (Chemical Propulsion), Liquid Rocket Engine Turbopump Inducers," NASA SP 8052, May 1971.

McConnaughey, P. K., Garcia, R., Griffin, L. A., Tucker, P. K., 1994, "Computational Fluid Dynamics (CFD) Consortium for Applications in Propulsion Technology (CAPT)," *Proceedings of the 1994 Conference on Advanced Earth-to-Orbit Propulsion Technology*, NASA CP-3282, R. J. Richmond and S. T. Wu, eds., May 17-19, Marshall Space Flight Center, AL, Vol. 2, pp. 63-70.

Shih, A. M., 1997, " Modification to the TIGER Grid Generator," Final Technical Report and User's Manual, NAS8-40849, April 4, 1997.

Steinbrenner, J.P., and Chawner, J.R., 1996, "Gridgen's Synergistic Implementation of CAD and Grid Geometry Modeling", from *Numerical Grid Generation in Computational Field Simulations*, ed. by Soni, B.K., Thompson, J.F., Hauser, Jochem, and Eiseman, Peter, publ. by Engineering Research Center for Computational Field Simulation, Mississippi State University, pp. 363-372.